



Developing and testing a computer vision method to quantify 3D movements of bottom-set gillnets on the seabed

Savina, Esther; Krag, Ludvig Ahm; Madsen, Niels

Published in:
ICES Journal of Marine Science

DOI (link to publication from Publisher):
[10.1093/icesjms/fsx194](https://doi.org/10.1093/icesjms/fsx194)

Publication date:
2018

Document Version
Accepted author manuscript, peer reviewed version

[Link to publication from Aalborg University](#)

Citation for published version (APA):
Savina, E., Krag, L. A., & Madsen, N. (2018). Developing and testing a computer vision method to quantify 3D movements of bottom-set gillnets on the seabed. *ICES Journal of Marine Science*, 75(2), 814-824.
<https://doi.org/10.1093/icesjms/fsx194>

General rights

Copyright and moral rights for the publications made accessible in the public portal are retained by the authors and/or other copyright owners and it is a condition of accessing publications that users recognise and abide by the legal requirements associated with these rights.

- Users may download and print one copy of any publication from the public portal for the purpose of private study or research.
- You may not further distribute the material or use it for any profit-making activity or commercial gain
- You may freely distribute the URL identifying the publication in the public portal -

Take down policy

If you believe that this document breaches copyright please contact us at vbn@aub.aau.dk providing details, and we will remove access to the work immediately and investigate your claim.

Developing and testing a computer vision method to quantify 3D movements of bottom-set gillnets on the seabed

Esther Savina^a, Ludvig Ahm Krag^a, Niels Madsen^{a*}

^a Technical University of Denmark, National Institute of Aquatic Resources, Willemoesvej 2, 9850 Hirtshals,
Denmark

* Section of Biology and Environmental Science, Department of Chemistry and Bioscience, Aalborg
University, Fredrik Bajers Vej 7, 9220 Aalborg, Denmark

CORRESPONDING AUTHOR

Esther Savina, esav@aqua.dtu.dk, +45 35 88 32 02

Technical University of Denmark, National Institute of Aquatic Resources, Willemoesvej 2,
9850 Hirtshals, Denmark

KEYWORDS:

Coastal waters; Environmental impact; Fishing gear; Gillnet; Habitat; Stereo vision

HIGHLIGHTS

- A stereo imaging method was adapted to quantify in situ fishing gear habitat effect.
- The movement of the leadline of light and heavy bottom gillnets on sand was assessed.
- The direct mechanical damage to the seabed (penetration) of gillnets was minimal.
- The sweeping movements were higher than estimated by experts, up to 2 m.
- Light nets were moving significantly more than heavy ones.

ABSTRACT

1 Gillnets are one of the most widely used fishing gears, but there is limited knowledge about
2 their habitat effects, partly due to the lack of methodology to quantify such effects. A stereo
3 imaging method was identified and adapted to quantify the dynamic behavior of gillnets in-
4 situ. Two cameras took synchronized images of the gear from slightly different perspectives,
5 allowing to estimate the distance from the observation unit to the gear such as in the human 3D
6 vision. The sweeping motion on the seabed and the penetration into the sediment of the leadline
7 of light and heavy commercial bottom gillnets deployed in sandy habitats in the Danish coastal
8 plaice fishery were assessed. The direct physical disruption of the seabed was minimal as the
9 leadline was not penetrating into the seabed. Direct damage to the benthos could however
10 originate from the sweeping movements of the nets, which were found to be higher than usually
11 estimated by experts, up to about 2 m. The sweeping movements were for the most part in the
12 order of magnitude of 10 cm, and resulted in a total swept area per fishing operation lower than
13 any of the hourly swept area estimated for active fishing gears. Whereas the general perception
14 is that heavy gears are more destructive to the habitat, light nets were moving significantly
15 more than heavy ones. The established methodology could be further applied to assess gear
16 dynamic behavior in-situ of other static gears.

17 **1. Introduction**

18 Ecosystem effects of fisheries and in particular habitat damage is of high interest in an
19 Ecosystem Approach to Fisheries as some fishing gears can remove or damage habitat forming
20 structures, potentially reducing the complexity, diversity and productivity of benthic
21 environments (Jennings and Kaiser, 1998; Kaiser *et al.*, 2000; Kaiser *et al.*, 2002; Hermsen *et*
22 *al.*, 2003; Grabowski *et al.*, 2014). The Marine Strategy Framework Directive defines seabed
23 integrity as one of the descriptors required by the European Union member states to ensure
24 Good Ecological Status (E.C., 2008). Methods are being developed for assessing the
25 responsiveness of different seabed habitats to fishing activities, resulting in habitat sensitivity
26 maps, which can be used in marine spatial planning (Eno *et al.*, 2013). Eco-labelling initiatives
27 have started to take gear impacts on habitats into account in their assessments (Olson *et al.*,
28 2014). In this context, providing documentation for the habitat effect of fishing gears is of prime
29 importance, especially for small-scale fisheries where maintaining profitability may be
30 challenging and where there are benefits to keeping fishing in traditional fishing grounds,
31 including sensitive areas, or where higher prices could be obtained from eco-labelling.

32 Gillnets stand as the fourth most important general gear type (out of 8) contributing to the
33 global marine catches (in weight, based on data from 1950 to 2001, Watson *et al.*, 2006). About
34 40% of the European fishing vessels belong to the small-scale bottom-set gillnets fleet (by
35 number, as of December 2016), with 33 644 active vessels under 12m with set gillnets (GNS) as
36 main gear, and up to 80% in Denmark for example (by number, with 1838 active vessels under
37 12m with GNS as main gear as of December 2016) (E.C., 2016). It is generally assumed that
38 habitat impacts of fixed gears are lower than those of mobile gears (Suuronen *et al.*, 2012;
39 Grabowski *et al.*, 2014). However, these conclusions are based on few experimental studies. For

40 example, there were only five studies regarding fixed gears, i.e., longlines, traps and gillnets, out
41 of 97 used for the latest assessment in New England, US (Grabowski *et al.*, 2014). Taking a
42 closer look at bottom gillnets, the lack of studies regarding habitat impact might be attributed to
43 the general assumption of negligible effects (Uhlmann and Broadhurst, 2013). However, after in
44 situ observation at two rocky reefs, Shester and Micheli (2011) identified set gillnets as a
45 priority conservation concern due to their potential to damage habitat-forming species. In the
46 Welsh part of the Irish Sea, Eno *et al.* (2013) assessed nets sensitivity as high to medium for
47 high to low fishing intensities in 8 habitats out of 31, mostly rock with associated branching
48 species such as kelp, seaweeds or maerl beds. There is no direct evidence of potential effect for
49 many of the current habitat-gear combinations, and the degree to which fixed gears drift on the
50 bottom has to be quantified for the different bottom types (Eno *et al.*, 2013; Grabowski *et al.*,
51 2014).

52 There is limited knowledge about the habitat effects of bottom gillnets partly due to historical
53 focus on active gears, but also because data collection and analysis calls for the development of
54 appropriate innovative assessment methodologies. Several optical or acoustic techniques have
55 been developed as complementary tools to assess the impact of mobile gears on the seabed
56 (Smith *et al.*, 2003; Humborstad *et al.*, 2004; O'Neill *et al.*, 2009; Lucchetti and Sala, 2012;
57 Depestele *et al.*, 2016). However, not all techniques provide a spatial resolution fine enough to
58 assess bottom gillnets. Others are restrictive in sampling duration. Eventually, not all techniques
59 can easily and safely be operated around bottom gillnets, prone to entanglement. Video offers
60 more precision and less bias than direct visual observation, as it is possible to view each
61 recording repeatedly or at lower speed (Neuswanger *et al.*, 2016). Nevertheless, the value of a
62 video recording as informative data also depends on the ability to extract relevant measurements

63 (Struthers *et al.*, 2015; Neuswanger *et al.*, 2016). Waterproof action cameras are now commonly
64 available tools to deliver cost efficient high-definition underwater video recordings (Struthers *et*
65 *al.*, 2015) using simple deployment platforms.

66 In bottom-set gillnets, the gear components in contact with the seabed are the headline, the
67 anchors and the bridle lines (connecting the anchors to the netting). Gillnets may be dragged on
68 the seabed and become tangled in bottom features as the gear moves with the water flow while
69 fully deployed on the seabed. Gillnets may also be snagged on benthic structures or organisms
70 during retrieval of the gear (Shester and Micheli, 2011). The gear characteristics and rigging
71 specifications play a key role in the net behavior, and therefore its potential seabed effects. The
72 net is spread vertically by the buoyancy of floats on the headline and weight in the headline
73 (Takagi *et al.*, 2007; He and Pol, 2010). The gear is usually moored at both ends with weights or
74 anchors, which can cause vertical and horizontal deformation of the netting (Shimizu *et al.*,
75 2007; He and Pol, 2010). Water flow pushes the netting to incline and bulge out of the vertical
76 plane (Stewart, 1988; Takagi *et al.*, 2007). Shimizu *et al.* (2007) calculated that the headline
77 would slide across the sea bottom if the force acting on the headline is larger than the coefficient
78 of static friction, but sliding motions of bottom gill nets during fishing have not been directly
79 observed in any study to our knowledge.

80 The aim of the study was to identify, adapt, test and use a suitable methodology for assessing
81 the dynamic behavior of the headline of bottom gillnets, i.e., the sweeping motion on the seabed
82 and the penetration into the sediment. An in-situ pilot experiment using stereo imaging was
83 carried out in the Danish gillnet coastal plaice fishery.

84 **2. Material and methods**

85 **Stereo imaging: general principle and quantitative measurements with VidSync**

86 Stereo imaging consists of two cameras taking synchronized images of a scene from slightly
87 different perspectives, or vantage points, which then allow to estimate the distance to an object
88 such as in the human 3D vision. If an object is uniquely identified in both images and if the
89 translation and rotation of one camera relative to the second is known, it is then possible to
90 estimate the location of the object in 3D space (Schmidt and Rzhanov, 2012).

91 The free open-source Mac application VidSync (www.vidsync.org) was developed based on
92 the OpenCV library computer vision algorithms by Neuswanger *et al.* (2016) to process stereo
93 video recordings. The mathematical calculations of 3D measurements and their application in
94 VidSync are detailed by Neuswanger *et al.* (2016).

95 Before the proper calculation of the 3D coordinates of a point, one has to correct for lens
96 distortion and establish the perspective of each camera. Lens distortion is induced by the fisheye
97 lens of the camera, meant to widen its angle of view, but particularly pronounced when the
98 camera records underwater through housing and prone to bias calculations. Correction factors,
99 or distortion parameters, can be found by locating nodes on a chessboard pattern or calibration
100 frame and arranging them into straight lines. The same chessboard pattern can be used to
101 calculate the projection matrices for each camera by matching the known physical 2D node
102 coordinates on each face of the calibration frame with screen coordinates, which are recorded in
103 VidSync by clicking on the centre of each node on the video recordings.

104 The 3D coordinates of a point are calculated in VidSync by iterative triangulation, aiming at
105 establishing two lines-of-sight that approximately intersect at the point of interest, which is
106 undertaken by clicking on the different points of the leadline, on each video recording. The

107 calibration frame is the only source of information on the scaling of distances from which
108 VidSync reconstructs a 3D space from the 2D video recordings.

109 **Pilot experiment: location of the sea trials, net type and gear specifications**

110 The pilot experiment took place in ICES area IIIa (Kattegat) off the coast of Northern
111 Denmark aboard a small research vessel (5 m) on September 10th 2015. Because of its
112 importance regarding Danish traditional commercial fishing grounds, and as the probability that
113 the headline would slide across the sea bottom is higher for smooth surfaces than for rough
114 surfaces (Shimizu *et al.*, 2007), the experiment took place on sandy bottom. Nets were deployed
115 in shallow waters, i.e., 1.5 to 3 m depth, to operate the observation units as best as possible in
116 relation to the deployed gillnets in the relatively turbid waters. Our experimental conditions
117 were at the lower depth range of commercial practices, but many coastal vessels participating in
118 the gillnet plaice fishery, usually fish between 2 and 8 m in the summer and autumn. All
119 observations were made away from the surf zone in calm weather to limit the influence of
120 waves.

121 Two different types of commercial bottom gillnets, light and heavy, were used to give a
122 gradient of commercial conditions. All nets were commercial plaice gillnets, and heavy and light
123 nets differed only in the specifications of the head- and leadlines (Table 1). The headline was
124 different for the two gear types as it influences the inclination of the net and has commonly more
125 buoyancy for heavier nets in commercial conditions. It is commercial practice to work with such
126 a net height when targeting plaice (1.1 m). Mesh size was selected according to the fish target at
127 the chosen trial location, i.e., plaice on sandy habitat. Both net types were made by Daconet
128 (www.daconet.dk) with the same manufacturing process.

129 **Pilot experiment: stereo recording units and their calibration**

130 Each observation unit was composed of a simple metallic frame made of 1 cm diameter steel
131 sticks (Fig. 1). Each metallic frame was ballasted with concrete poured in 7.5 cm diameter and
132 12.5 cm long polyvinyl chloride (PVC) tubes at each foot. The use of a light frame ensured a
133 surface as small as possible for limiting drag, whereas the heavy feet guaranteed that the frame
134 would remain in position when lowered on the seabed. Two cameras in their waterproof housing
135 were mounted on the frame at a distance of 65 cm from each other and protected by netting (Fig.
136 1). The use of netting aimed at preventing entanglement of the netting of the gillnet into the
137 frame when in contact. Cameras were GoPro Hero 3 and 3+ cameras, each pair of a recording
138 unit having identical settings (type of camera and video mode). For all fleets, the video
139 resolution was set to 1080p SuperView, i.e., the sides of the video were stretched out for greater
140 viewing, the frame per second was set to 30, and the field of view was set to Ultra Wide. Initial
141 testing of the set-up with resolution set to 4K and frame per second set to 12 resulted in
142 measurement errors exceeding 25%.

143 A 3D calibration frame of 80 x 51 x 31 cm with a 9-by-15 node pattern in the front face and
144 an 8-by-5 node pattern in the back face was used (Fig. 2). The front face was made of perspex
145 acrylic glass (PMMA) (<http://vink.dk/>), which can refract light when looking at the back frame
146 and slightly change the apparent position of the nodes (Neuswanger *et al.*, 2016). A correction
147 was applied to compensate for light refraction by the front frame based on the thickness of the
148 material (35mm), the refractive index of the material (PMMA, 1.491), and the refractive index
149 of the medium (salt water, 1.342) (Neuswanger *et al.*, 2016).

150 Each observation unit, consisting of two cameras mounted on a metallic frame was submerged
151 in water and calibrated at the Nordsøen Oceanarium (<http://nordsoenoceanarium.dk/>).

152 **Pilot experiment: experimental set-up and measurement of water flow speed**

153 Three individual net panels were attached at the floatlines to form a fleet, similar to
154 commercial practice (Fig. 3a). All fleets were set in a straight line parallel to the coast and the
155 predominant current direction. Fleets were anchored at both ends with four kg anchors using six
156 metres bridle lines following commercial practices. As the motion at a specific section of the net
157 depends on its relative position (Shimizu *et al.*, 2004), each stereo recording unit was positioned
158 on the seabed facing the middle length of the fleet, i.e., the part of the net the most likely to slide
159 assuming that the nets are set in a straight line, at about 1 to 2 m from the net (Fig. 3b). Three
160 fleets were soaked at the same time for two to three hours during the day. Fleets soaked together
161 formed a run. Data was collected while the gear was fully deployed on the seabed.

162 Nets were marked with different red tape patterns on the leadline to ensure that these marks
163 would easily be uniquely identified on the video recordings (Fig. 3 and 4). A high resolution
164 clock (B. Lundgren, pers. comm.) was recorded at the beginning of every recording, providing a
165 distinctive feature to synchronize the video recordings from the left and right cameras to the
166 nearest video frame.

167 The water speed was recorded using two sets of a GPS device (GP-102,
168 www.canmore.com.tw) attached to a buoy and left drifting during data collection (Fig. 5). A
169 holed PVC tube with attached lead hanging from the buoy was used to make sure that the
170 measurement gave the current speed in the water column and not at the surface (wind drift). Use
171 of the flow speed average from the bottom up to the net height could lead to more precise
172 calculation by incorporating vertical difference in flow speed caused by the bottom boundary
173 layer, but it is commonly accepted to use the current speed measured at the median net height in

174 the mid-point location between the nets (Matuda and Sannomiya, 1977a, b; Matuda and
175 Sannomiya, 1978; Matuda, 1988; Shimizu *et al.*, 2007).

176 Hourly instantaneous horizontal seawater velocities (2D) at 1m depth were also extracted
177 from the Forecasting Ocean Assimilation Model 7 km Atlantic Margin model (FOAM AMM7)
178 (EU Copernicus, 2017). The 7 km resolution of the model restricts its utility in the coastal zone
179 where strong sub-grid scale variability in shallow water bathymetry affects the wave field, and
180 modelled data was therefore used as an overall indication of water flow speed in the area, but
181 not for instantaneous measurement at each net position.

182 **Pilot experiment: data analysis**

183 The position of the calibration frame defined the 3D coordinate system, i.e., the origin (0, 0,
184 0) was the bottom left point on the front face of the calibration frame, the front and back faces
185 were found in the x - z plane, with the front face in the plane $y=0$ and the back face in the plane
186 y =distance between both faces (Fig. 2). Thus, the net movements in the X dimension were
187 positive when the net moved rightward or negative leftward (Fig. 4). The movements in the Y
188 dimension were positive when the net moved backward or negative forward. As the observation
189 units were facing the coast during deployment, the movements in the Y dimension were positive
190 when the net moved towards the coast and negative towards the open sea. The movements in the
191 X and Y dimensions represent the sweeping motion of the net. The movements in the Z
192 dimension were positive when the net moved upward, i.e., lifting off the seabed, or negative
193 downward, i.e., dropping on the seabed. The movements in the Z dimension represent the seabed
194 penetration.

195 We checked for data entry mistakes or calibration problems by examining diagnostic error
196 measures provided for each 3D point by Vidsync (Neuswanger *et al.*, 2016). To quantify actual

197 errors in 3D measurements, the calculated (VidSync) and measured (measuring tape) distances
198 between two nodes as well as between the two faces of the calibration frame were compared in a
199 first control test, and the calculated and measured distances between two coloured threads on the
200 leadline of both light and heavy gillnets were compared in a second control test. The first point
201 calculated was set as a reference starting point with a given position of zero in the three
202 dimensions, and the position value of this reference point was subtracted from the position
203 values of the following points. The dynamic behavior of the leadline was analysed using a
204 simple motion metrics in the three spatial dimensions, i.e., the maximum distance covered by the
205 leadline in each dimension, calculated as the difference between the maximum and the minimum
206 position values of each mark.

207 Significant differences between light and heavy net configurations were tested for as follows.
208 Data exploration was applied following Zuur *et al.* (2010). The effect of net configuration (light
209 or heavy), run (I or II) and dimension (X, Y or Z) on the maximum movement of the leadline
210 was initially modelled as a linear regression model containing sensible interactions based on
211 experimental knowledge and data exploration as in model (1). A log-transformation was applied
212 on the response variable as a solution to heterogeneity of variance. As the video recording
213 duration varied between marks (Table 2), duration was used as an offset. The linear regression
214 model is given by:

$$215 \log(Y_i) = \beta (\text{Dimension}_i, \text{Net}_i, \text{Run}_i) + 1 * \log(\text{Duration}_i) + \varepsilon_i \text{ with } \varepsilon_i \sim N(0, \sigma_i^2) \quad (1)$$

216 where Y_i is the maximum movement of the i th mark, β is the population slope and ε_i is the
217 residual normally distributed with expectation 0 and variance σ_i^2 .

218 Model selection was applied to model (0) by dropping individual explanatory variables one by
219 one based on hypothesis testing (F-statistic), and resulted in the preferred model (2):

$$220 \log(Y_i) = \beta (\text{Dimension}_i) + \gamma (\text{Net}_i, \text{Run}_i) + 1 * \log(\text{Duration}_i) + \varepsilon_i \text{ with } \varepsilon_i \sim N(0, \sigma_i^2) \quad (2)$$

221 All parameters were tested significant at p-value <0.001. The four assumptions that allow the
222 sample data to be used to estimate the population data are: normality, homogeneity,
223 independence and fixed explanatory variable (i.e., measurement error in the explanatory variable
224 is small compared to the noise in the response variable). The chosen model (2) was validated by
225 visual inspection of the residuals.

226 The video recordings were processed with VidSync version 1.66 (www.vidsync.org). All
227 other analyses were performed by the open-source software R 3.2.3 (R Core Team, 2016).

228 3. Results

229 Data collected and error measures

230 Video recordings from five fleets were clear and long enough for analysis, i.e., three fleets for
231 run I and two fleets for run II (Table 2). Nets were deployed at 3 and 1.5-2 m depth,
232 respectively, for runs I and II. All video recordings were collected in good weather and sea
233 conditions. Modelled hourly water velocities were (average \pm standard deviation) 0.049 ± 0.003
234 and 0.031 ± 0.027 m.s⁻¹, respectively, for runs I and run II, which was in agreement with
235 measured water velocities of 0.028 ± 0.025 m.s⁻¹ for run II. A total of eight marks could be
236 uniquely identified on the leadline, i.e., one mark for fleet Ia, Ib, IIa, two marks for fleet Ic and
237 three marks for fleet IIb (Table 2). Total video recordings duration per mark ranged from 13 to
238 138 minutes, with an average of (mean \pm standard deviation) 73 ± 84 min for light nets and 109

239 ± 41 min for heavy nets (Table 2). An extract of one of the recordings is given as an example
240 (supplementary material).

241 Diagnostic error measures provided for each 3D point by Vidsync did not show any data
242 entry mistake or calibration problem.

243 Distortion corrections reduced the distortion error, i.e., the distance between the input screen
244 points and the reprojected screen points, by (mean \pm standard deviation) $54 \pm 12\%$ for all cameras
245 in all recording units. The remaining distortion per point was 0.94 ± 0.21 pixels on average for
246 all cameras in all recording units. There was a slight increase in absolute error for calculations
247 near the edge or centre of the screen for some of the video recordings.

248 In the first control test, the calculated (Vidsync) and measured (measuring tape) distances
249 between two nodes as well as between the two faces of the calibration frame were compared.
250 The Vidsync calculated distances were quite close to the measurements of the real distances,
251 with on average all measurement errors smaller than 10% (Fig. 6a).

252 In a second control test, the calculated (Vidsync) and measured (measuring tape) distances
253 between two coloured threads on the leadline of three light and four heavy gillnets were
254 compared. The Vidsync calculated distances were quite close to the measurements of the real
255 distances, with on average all measurement errors smaller than 25% (Fig. 6b). However, overall,
256 measurement errors for heavy nets in run I were up to around 150%, underestimating the
257 calculated distances compared to the measured ones.

258 Based on in-situ stereo vision measurements, the presented methodology can quantify the
259 dynamic behavior of the leadline of commercial bottom gillnets gillnet.

260 **Dynamic behaviour of the leadline and maximum distance covered by the leadline**

261 Marks were either stationary, e.g., mark 1 in the Y dimension, moved regularly continuous,
262 e.g., mark 1 in the X dimension, or moved with a sudden step, e.g., mark 6 in the X and Y
263 dimension (Fig. 7). Overall, marks on the same net moved similarly, e.g., marks 3 to 5 on fleet
264 Ic, even though local disparities were found, e.g., marks 7 and 8 on fleet IIb (Fig. 7). When
265 moving, all marks moved in a single direction in all dimensions, e.g., to the right only for mark
266 1 or to the left only for mark 6 (Fig. 7). However, not all fleets moved in the same direction, e.g.,
267 not all moved leftwards or towards the coast (Fig. 7).

268 The leadline was moving but not penetrating into the seabed as seen from the recorded
269 images, downward movements as calculated values in the Z dimension being most likely due to
270 slight disparities in the seabed features. The leadline was apparent in most of the footages,
271 except in rare occasions in which about five cm in length were not visible. The sea bottom was
272 slightly bumpy and it was not possible to see if the leadline was covered by sand or only behind
273 a bump in these few occasions.

274 The maximum distance covered by each mark on the leadline ranged from 0.14 to 1.10m,
275 0.06 to 2.01m and 0.02 to 0.26m in the X, Y and Z dimensions, respectively, with an average of
276 (mean \pm standard deviation) 0.96 (\pm 0.20) for light and 0.31 (\pm 0.15) m for heavy nets, 1.5 (\pm 0.67)
277 for light and 0.38 (\pm 0.25) m for heavy nets, and 0.14 (\pm 0.17) for light and 0.06 (\pm 0.03) m for
278 heavy nets, in the X, Y and Z dimensions, respectively (Table 2). The maximum swept area
279 covered by the movements of each observed mark (X and Y dimensions) ranged from 0.02 to
280 1.65m², with an average of 1.41 (\pm 0.34) and 0.13 (\pm 0.15) m² for light and heavy nets,
281 respectively (Table 2). The leadline movements in the three dimensions were found to be
282 significantly different, with larger maximum movements in the Y dimension (Table 3).

283 Whatever the net type, the leadline moved 1.14 (0.49-2.65) times more in the Y dimension
284 (backward-forward) than in the X dimension (rightward-leftward), and 7.30 (3.15-16.89) times
285 more in the Y than in the Z dimension (upward-downward) (Fig. 8).

286 **Differences between net types and runs**

287 The leadline movements were significantly different for the two tested net configurations: for
288 both runs, light nets were moving more than heavy nets (Table 3). Whatever the dimension, light
289 nets moved 32.53 (95% confidence limits: 11.01-96.09) times more than heavy nets in run I, and
290 1.41 (0.43-4.61) in run II (Fig. 8). A significant interacting effect of runs (Table 3) was found,
291 with both light and heavy nets moving more in run I than run II. Light nets moved 26.79 (6.81-
292 105.47) times more in run I than in run II, and heavy nets moved 1.16 (0.50-2.68) times more in
293 run I than in run II. This is in line with higher water velocities in run I compared to run II.

294 **4. Discussion**

295 **Stereo-imaging for quantifying gear dynamic behavior in-situ**

296 The dynamic behavior of the leadline of commercial bottom gillnets could be quantified in
297 details using the presented methodology based on measurements of in-situ stereo vision
298 recordings. The methodology quantify both the seabed penetration and sweeping motion of the
299 leadline. This methodology can be further applied to assess habitat effect of other gear types,
300 especially other static gears such as creels and pots, or more generally further assess gear
301 dynamic behavior in-situ. Indeed, as net geometry affects the gear selectivity, an improved
302 understanding of the gear dynamic behavior would provide a better insight into the capture
303 process (Shimizu *et al.*, 2004; Herrmann *et al.*, 2009).

304 The stereo-imaging experimental set-up, i.e., the choice of camera separation and the
305 dimensions and position of the calibration frame, was configured to measure relatively small
306 objects close to the cameras. Accuracy and precision decreased as distance from the cameras
307 increased. The nets were not expected to move in such an order of magnitude, but a larger
308 chessboard, i.e., large enough to fill the screen, could have helped limit our measurement errors.
309 The fish eye effect could be reduced by limiting the field of view (instead of choosing ultra wide
310 setting).

311 A variety of challenges were faced when deploying the observation units near the nets at sea,
312 among which water turbidity, also noticed as a limitation for optical methods by Lucchetti and
313 Sala (2012) and Struthers *et al.* (2015). The video recordings could also appear blurry due to the
314 scattering effects of particles in the water column, and images could be exposed differently from
315 the two cameras due to irregular lightning and displacement between the cameras (Schmidt and
316 Rzhanov, 2012). These optical limitations reduced the number of recorded images that could be
317 processed. A camera that only captures light reflected from objects further away than a certain
318 distance could be used to remove the effects of scattered light and therefore solve the issue of
319 water turbidity (under development, L.A. Krag, pers. comm.).

320 Calibration and distortion corrections obtained in a tank were used for processing the in-situ
321 video recordings. The same camera specifications, i.e., camera settings and relative orientation,
322 for each recording unit, were used but any optical adjustment such as removing a camera from
323 its underwater housing to change a battery or a change of the angle between the cameras during
324 transportation/aboard the vessel may have affected the parameters and therefore the results. The
325 control tests did not show major issues, and one can therefore rely on the order of magnitude of

326 the results. But, the cameras should remain fixed throughout the experiment in a later use of the
327 stereo-imaging method.

328 **Pilot estimation of gillnets 3D dynamic behaviour and their seabed effects**

329 The leadline of bottom gillnets, fully deployed on the bottom, could sweep the seabed in
330 sandy habitats up to about 2 m, for the most part in the order of magnitude of 10 cm.
331 Movements were either continuous or in a sudden step, which was different from the periodical
332 displacement observed by Shimizu *et al.* (2004). This could be due to a different initial net shape
333 and spread of the leadline for each fleet when reaching the sea bottom (Shimizu *et al.*, 2007), or
334 local water flow disparities. The in-situ measurements of the leadline showed that movements
335 were the smallest in the Z dimension, less than a few centimeters. The leadline was moving but
336 not penetrating into the seabed as seen from the recorded images, downward movements as
337 calculated values in the Z dimension being most likely due to slight disparities in the seabed
338 features.

339 In terms of seabed disturbance, this means that the physical disruption of the seabed
340 (penetration) of gillnets is minimal compared to the sweeping of the gear, whereas seabed
341 penetration was observed as partly responsible for habitat physical impact in active fishing gears
342 (Eigaard *et al.*, 2016; Depestele *et al.*, 2016). The potential direct damage to the benthos would
343 therefore originate from the sweeping movements of the gillnets, as the leadline and netting can
344 snag and entangle available entities. The sweeping movements of plaice gillnets in the Danish
345 fishery were found to be higher than usually estimated by experts, but cannot be compared to
346 other in-situ measurements as these are the first quantitative measurements to our knowledge. A
347 maximum of 30 kms of nets are soaked in a typical bottom-set gillnets fishing operation
348 (Montgomerie, 2015). The swept area can roughly be estimated to about 0.04 km² for light nets

349 and 0.01 km² for heavy nets (based on a rectangle area calculation using the average measured
350 range per mark in the Y dimension as presented above, i.e., 1.5 for light and 0.38 m for heavy
351 nets). This is lower than any of the hourly swept area estimated for active fishing gears by
352 Eigaard *et al.* (2016), ranging from 0.05 km² for beam trawl to 1.5 km² for Scottish seining
353 surface impact. However, the swept area of an active gear is swept once by the gear, whereas
354 passive gear are likely to sweep the same area multiple times. The measured movements were
355 representative only to a certain point of what really happens: as the nets were getting too far
356 from or too close to the recording unit, it was not possible to take measurements anymore. The
357 present measurements of the movement of the leadline are therefore underestimated. However,
358 the movement of the leadline was not unlimited as the fleets were anchored on the bottom. For
359 the same reason, a major difference between longer soak durations on the estimated swept area
360 was not expected.

361 The dynamic behavior of the leadline was analysed using a simple motion metrics in the three
362 spatial dimensions, i.e., the maximum distance covered by the leadline in each dimension.
363 However, how fast the leadline moves is also expected to play a key role in the assessment of
364 the potential effects of the leadline movement on the seabed. Indeed, the fastest movements of
365 the leadline are the ones most likely to cause damage. As observed previously, marks moved
366 either regularly continuous, or with a sudden step, and speed was therefore not a good indicator.
367 Further assessment should include a spatio-temporal trajectory analysis, with focus on
368 acceleration, i.e, change in velocity with time.

369 The observations of the pilot project only covered the soaking phase of a gillnetting operation,
370 i.e., when the gear was fully deployed on the bottom, and not the retrieval of the gear, therefore
371 not covering the total potential habitat effect of bottom gillnets. Shester and Micheli (2011)

372 observed the entanglement and removal of kelp plants and gorgonian corals by set gillnets while
373 being hauled. Effects of hauling are more likely to be destructive as more power is exerted
374 through the nets (hauler) than when soaking, for which, e.g., a stone could eventually stop the
375 net. It is however known from fishermen practices that the way the gear is handled when hauling
376 can significantly reduce possible habitat damage, e.g., hauling in the current direction.

377 **Gear configuration as mitigation measure**

378 As demonstrated in this experiment, the gear configuration affects the sweeping of the nets,
379 with light nets moving significantly more than heavy ones. Whereas the general perception is
380 that heavy gears are more destructive to the habitat, such as in active gears (Kaiser *et al.*, 2002),
381 it was demonstrated here that a heavier leadline would result in less movement, being the actual
382 issue in terms of potential habitat damage of bottom-set gillnets. Therefore, gear configuration
383 has a strong mitigation effect regarding the sweeping behavior of the leadline, and habitat
384 damage could be reduced by using nets mounted with heavier leadlines.

385 In addition to the tested net configuration, i.e., light and heavy nets, other components of the
386 fishing gear in gillnets could be looked at to mitigate their habitat effects. Bridles attached to the
387 head or bottom line will give the netting different types of curves which will affect the drag
388 (Stewart and Ferro, 1985). Twine diameter, mesh size, netting hanging ratio and length of fleets,
389 as well as the way the nets are set out could also affect the drag and therefore the leadline
390 movement of bottom-set gillnets.

391 **General applicability of the results**

392 Due to the limited number of observations and choice of model, movement values presented
393 here were not meant to be predicted outside of the experimental conditions. Water flow speeds
394 during data collection were lower than the average range in coastal Danish waters (0.26 to

395 0.77m.s⁻¹) (National Geospatial-Intelligence Agency, 2013). Therefore, such experimental
396 conditions of mild sea conditions gave conservative estimates. The flow from waves, induced by
397 wind, and current, induced by both tides and wind, represents the most common flow condition
398 on the seabed for shallow water depths at our scales of interest (spatial and temporal) (Jensen
399 and Jónsson, 1987; Otto *et al.*, 1990; Myrhaug, 1995; Soulsby, 1997). The complex effects of
400 water flow, waves and wind, can change at a small scale, and influence the behavior of the gear
401 (Shimizu *et al.*, 2004). These local differences in water flow could be a reason for the significant
402 interacting effect of runs. When moving, all marks moved in a single direction in all dimensions,
403 which indicated that movements were not caused by the local action of waves, i.e., flow and
404 surge which would have resulted in, e.g., repeated forward-backward movements. When
405 moving, not all fleets moved in the same direction, which indicated that movements were not
406 caused by the overall action of waves, i.e., towards the coast. Detailed measurement of the
407 current direction and speed in further experiments could provide with a better understanding of
408 the environmental variables at stake. Very shallow waters were needed to test how to operate the
409 camera cages, and also because water was turbid at the time of data collection. Further
410 estimations should be run in deeper waters for which water flow conditions would be different,
411 as the turbulent boundary layer does not occupy the entire water column contrary to shallow
412 waters (Soulsby, 1997; Otto *et al.*, 1990). This is conditioned on an improved method that
413 allows to place an observation unit quite close to the net at such depths, e.g., using a sonar, and
414 external lightning to compensate for the reduced light conditions.

415 Because the pilot project was located in very shallow waters, a small net height was chosen. It is
416 commercial practice to work with such a net height, but higher nets may have an influence on

417 the overall gear equilibrium and drag. So may caught fish, but it is generally assumed that fish
418 would not have a great effect (Shimizu *et al.*, 2007).

419 **Supplementary material**

420 An extract of one of the video recordings is given as supplementary material at ICESJMS
421 online.

422 **Acknowledgements**

423 The authors wish to thank Bo Lundgren, Reinhardt Jensen, Søren Larsen Grønby and Aage
424 Thaarup from DTU Aqua, for their help with the calibration and experiment at sea. The authors
425 also wish to thank Martin Riis from the Nordsøen Oceanarium for use of the tank and Jason
426 Neuswanger for help with Vidsync. Finn Larsen (DTU Aqua) made valuable comments on the
427 manuscript and Anders Nielsen (DTU Aqua) assisted in the statistical analysis of the data. The
428 Ministry of Environment and Food of Denmark funded the present study as part of the
429 ‘Skånfisk’ project, but was not involved in the conduct of the research or preparation of the
430 article.

431 **References**

432 Depestele, J., Ivanović, A., Degrendele, K., Esmaceli, M., Polet, H., Roche, M., Summerbell, K.,
433 Teal, L.R., Vanellander, B., O’Neill, F.G. 2016. Measuring and assessing the physical
434 impact of beam trawling. ICES Journal of Marine Science, 73: i15-i26.

435 E.C. 2008. Directive 2008/56/EC of the European Parliament and of the Council of 17 June
436 2008 establishing a framework for community action in the field of marine environmental
437 policy (Marine Strategy Framework Directive).

- 438 E.C. 2016. Community Fishing Fleet Register Data Base. Available from
439 <http://ec.europa.eu/fisheries/fleet/index.cfm> [Accessed on January 11th 2017].
- 440 Eigaard, O.R., Bastardie, F., Breen, M., Dinesen, G.E., Hintzen, N.T., Laffargue P., Mortensen,
441 L.O., Nielsen, J.R., Nilsson, H.C., O'Neill, F.G., Polet, H., Reid, D.G., Sala, A., Sköld, M.,
442 Smith, C., Sorensen, T.K., Tully, O., Zengin, M., Rijnsdorp, A.D. 2016. Estimating seabed
443 pressure from demersal trawls, seines, and dredges based on gear design and dimensions.
444 ICES Journal of Marine Science, 73: i27-i43.
- 445 Eno, N.C., Frid, C.L.J., Hall, K., Ramsay, K., Sharp, R.A.M., Brazier, D.P., Hearn, S., Dernie,
446 K.M., Robinson, K.A., Paramor, O.A.L., Robinson, L.A. 2013. Assessing the sensitivity of
447 habitats to fishing: from seabed maps to sensitivity maps. Journal of Fish Biology, 83: 826-
448 846.
- 449 EU Copernicus, 2017. Atlantic - European North West Shelf - Ocean Physics Analysis and
450 Forecast (NORTHWESTSHELF_ANALYSIS_FORECAST_PHYS_004_001_b). Available
451 from EU Copernicus Marine Service Information [http://marine.copernicus.eu/services-](http://marine.copernicus.eu/services-portfolio/access-to-products/?option=com_csw&view=details&product_id=NORTHWESTSHELF_ANALYSIS_FORECAST_PHYS_004_001_b)
452 [portfolio/access-to-](http://marine.copernicus.eu/services-portfolio/access-to-products/?option=com_csw&view=details&product_id=NORTHWESTSHELF_ANALYSIS_FORECAST_PHYS_004_001_b)
453 [products/?option=com_csw&view=details&product_id=NORTHWESTSHELF_ANALYSIS](http://marine.copernicus.eu/services-portfolio/access-to-products/?option=com_csw&view=details&product_id=NORTHWESTSHELF_ANALYSIS_FORECAST_PHYS_004_001_b)
454 [_FORECAST_PHYS_004_001_b](http://marine.copernicus.eu/services-portfolio/access-to-products/?option=com_csw&view=details&product_id=NORTHWESTSHELF_ANALYSIS_FORECAST_PHYS_004_001_b) [Accessed June 9th 2017]
- 455 Grabowski, J.H., Bachman, M., Demarest, C., Eayrs, S., Harris, B.P., Malkoski, V., Packer, D.,
456 Stevenson, D. 2014. Assessing the vulnerability of marine benthos to fishing gear impacts.
457 Reviews in Fisheries Science, 22: 142-155.

- 458 He and Pol, 2010. Fish behavior near gillnets: capture processes and influencing factors.
459 Behavior of Marine Fishes: Capture Processes and Conservation Challenges, Wiley-
460 Blackwell, pp. 183-203.
- 461 Hermesen, J.M., Collie, J.S., Valentine, P.C. 2003. Mobile fishing gear reduces benthic
462 megafaunal production on Georges Bank. Marine Ecology Progress Series, 260: 97-108.
- 463 Herrmann, B., Krag, L.A., Frandsen, Madsen, N., Lundgren, B., Stæhr, K.-J., 2009. Prediction
464 of selectivity from morphological conditions: methodology and a case study on cod (*Gadus*
465 *morhua*). Fish. Res., 97, 59-71.
- 466 Humborstad, O.-B., Nøttestad, L., Løkkeborg, S., Rapp, H. T. 2004. Rox-Ann bottom
467 classification system, sidescan sonar and video-sledge: spatial resolution and their use in
468 assessing trawling impacts. ICES Journal of Marine Science, 61: 53-63.
- 469 Jennings, S., Kaiser, M.J. 1998. The effects of fishing on marine ecosystems. Advances in
470 Marine Biology, 34: 201–212, 212e, 213–352.
- 471 Jensen, T.G., Jónsson, S. 1987. Measurement and analysis of currents along the Danish west
472 coast. Deutsche Hydrografische Zeitschrift, 40: 193–213.
- 473 Kaiser, M.J., 1998. Significance of bottom-fishing disturbance. Conservation Biology, 12:
474 1230–1235.
- 475 Kaiser, M.J., Spence, F.E., Hart, P.J.B., 2000. Fishing-gear restrictions and conservation of
476 benthic habitat complexity. Conservation Biology, 14: 1512-1525.
- 477 Kaiser, M.J., Collie, J.S., Hall, S.J., Jennings, S., Poiner, I.R. 2002. Modification of marine
478 habitats by trawling activities: prognosis and solutions. Fish and Fisheries, 3: 114-136.

- 479 Lucchetti, A., Sala, A. 2012. Impact and performance of Mediterranean fishing gear by side-
480 scan sonar technology. *Canadian Journal of Fisheries and Aquatic Sciences*, 69: 1806-1816.
- 481 Matuda, K. 1988. Headline height of bottom gill nets set across a water flow. *Fisheries*
482 *Research*, 6: 167–179.
- 483 Matuda, K. Sannomiya 1977a. Theory and design of bottom drift net. 2. Results of numerical
484 analysis on motion of gear. *Bulletin of the Japanese Society of Scientific Fisheries*, 43: 679–
485 687.
- 486 Matuda, K. Sannomiya, N. 1977b. Theory and design of bottom drift net. 1. Method of
487 numerical analysis on motion of gear. *Bulletin of the Japanese Society of Scientific Fisheries*,
488 43: 669–678.
- 489 Matuda, K. Sannomiya, N. 1978. Theory and design of bottom drift net. 3. Analytical solutions
490 of equation of motion of gear. *Bulletin of the Japanese Society of Scientific Fisheries*, 44: 7–
491 13.
- 492 Montgomerie, M., 2015. *Basic fishing methods*. Ed. by R. Forbes. Seafish, Edinburgh. 104 pp.
- 493 Myrhaug, D. 1995. Bottom friction beneath random waves. *Coastal Engineering*, 24: 259–273.
- 494 National Geospatial-Intelligence Agency of the United States Government, 2013. *Sailing*
495 *directions for Skagerrak and Kattegat*. 14th ed., 168p.
- 496 Neuswanger, J., Wipfli, M.S., Rosenberg, A.E., Hughes, N.F. 2016. Measuring fish and their
497 physical habitats: versatile e2D and 3D video techniques with user-friendly software.
498 *Canadian Journal of Fisheries and Aquatic Sciences*, 73: 1861–1873.

- 499 Olson, J., Clay, P.M., da Silva, P.P. 2014. Putting the seafood in sustainable food systems.
500 Marine Policy, 43: 104-111.
- 501 O'Neill, F.G., Summerbell, K., Breen, M. 2009. An underwater laser stripe seabed profiler to
502 measure the physical impact of towed gear components on the seabed. Fisheries Research,
503 99: 234-238.
- 504 Otto, L., Zimmerman, J.T.F., Furnes, G.K., Mork, M., Saetre, R., Becker, G. 1990. Review of
505 the physical oceanography of the North Sea. Netherlands Journal of Sea Research, 26: 161–
506 238.
- 507 R Core Team. 2016. R: A language and environment for statistical computing. R Foundation for
508 Statistical Computing, Vienna, Austria.
- 509 Schmidt, V.E., Rzhanov, Y. 2012. Measurement of micro-bathymetry with a GOPRO
510 underwater stereo camera pair. 2012 Oceans, IEEE, pp. 6404786.
- 511 Shester, G., and Micheli, F. 2011. Conservation challenges for small-scale fisheries: bycatch and
512 habitat impacts of traps and gillnets. Biological Conservation, 144: 1673-1681.
- 513 Shimizu, T., Takagi, T., Suzuki, K., Hiraishi, T., Yamamoto, K. 2004. Refined calculation
514 model for NaLA, a fishing net shape simulator, applicable to gill nets. Fisheries Science, 70:
515 401-411.
- 516 Shimizu, T., Takagi, T., Korte, H., Hiraishi, T., Yamamoto, K. 2007. Application of NaLA, a
517 fishing net configuration and loading analysis system, to bottom gill nets. Fisheries Science,
518 73: 489-499.

- 519 Smith, C.J., Rumohr, H., Karakassis, I., Papadopoulou, K.-N. 2003. Analysing the impact of
520 bottom trawls on sedimentary seabeds with sediment profile imagery. *Journal of Experimental*
521 *Marine Biology and Ecology*, 285-286: 479-496.
- 522 Soulsby, R. 1997. *Dynamics of marine sands: A manual for practical applications*. London:
523 Telford, 249p.
- 524 Stewart, P.A.M. 1988. Measurements of the effects of tidal flow on the headline heights of
525 bottom-set gillnets. *Fisheries Research*, 6: 181-189.
- 526 Stewart, P.A.M., Ferro, R.S.T. 1985. Measurements on gill nets in a flume tank. *Fisheries*
527 *Research*, 3: 29-46.
- 528 Struthers, D.P., Danylchuk, A.J., Wilson, A.D.M., Cooke, S.J. 2015. Action cameras: bringing
529 aquatic and fisheries research into view. *Fisheries*, 40: 502-512.
- 530 Suuronen, P., Chopin, F., Glass, C., Løkkeborg, S., Matsushita, Y., Queirolo, D., Rihan, D.
531 2012. Low impact and fuel efficient fishing - Looking beyond the horizon. *Fisheries*
532 *Research*, 119-120: 135-146.
- 533 Takagi, T., Shimizu, T., Korte, H. 2007. Evaluating the impact of gillnet ghost fishing using a
534 computational analysis of the geometry of fishing gear. *ICES Journal of Marine Science*, 64:
535 1517-1524.
- 536 Uhlmann, S.S., and Broadhurst, M.K. 2013. Mitigating unaccounted fishing mortality from
537 gillnets and traps. *Fish and Fisheries*, 16: 183-229.
- 538 Watson, R., Revenga, C., Kura, Y. 2006. Fishing gear associated with global marine catches. I.
539 Database development. *Fisheries Research*, 79: 97-102.

- 540 Zuur, A.F., Ieno, E.N., Elphick, C.S. 2010. A protocol for data exploration to avoid common
541 statistical problems. *Methods in Ecology and Evolution*, 1: 3-14.

Accepted manuscript

Table 1. Specifications of individual net panels used in the experimental set-up for light and heavy gear types. Height is given as stretched height. Headline and leadline types are given as specified by the net maker Daconet (firm's internal specification without unit). Specifications differing between the two gear types, light and heavy, are emphasized in bold.

Gear specifications		Light	Heavy
Net	Type	Gillnet	
	Target species	Plaice	
Twine	Diameter	0.30 mm	
	Type	Monofil	
	Material	Nylon	
	Knot	Double	
Mesh size	Nominal (bar length)	68 mm	
Dimensions	Height (mesh depth)	1.1 m (8.5)	
	Length (knot length)	82 m (4800)	
	Hanging ratio	25%	
Headline	Type (Hau Line mono)	1.5	2.5
	Buoyancy per 100 m	600 g	1200 g
Leadline	Type (Hau sinkline lead-free)	1.5	3
	Weight per 100 m	3.9 kg	11 kg

Accepted manuscript

Table 2. Run, fleet and net type for each of the eight marks on the leadline of gillnets observed in the pilot sea trial. Clip gives the total duration in min of the recorded images for each observed mark. The maximum distance (Max. distance) gives the maximum distance in m covered by the movements of each observed mark in the X, Y and Z dimensions. The maximum swept area (Max. swept area) gives the maximum swept area in m² covered by the movements of each observed mark in the X, Y and Z dimensions.

Mark	Run	Fleet	Net type	Clip (min)	Max. distance (m)			Max. swept area (m ²)
					X	Y	Z	
1	I	Ia	Heavy	125	0.32	0.19	0.05	0.06
2	I	Ib	Light	13	0.82	2.01	0.26	1.65
3	I	Ic	Heavy	128	0.30	0.44	0.07	0.13
4	I	Ic	Heavy	133	0.59	0.73	0.12	0.43
5	I	Ic	Heavy	101	0.21	0.56	0.06	0.12
6	II	IIa	Light	132	1.10	1.06	0.02	1.17
7	II	IIb	Heavy	29	0.14	0.29	0.04	0.04
8	II	IIb	Heavy	138	0.29	0.06	0.03	0.02

Accepted manuscript

Table 3. Estimates and standard errors (se) of the parameters in the chosen model for the log expected maximum movement of the leadline. All parameters were tested significant at p-value <0.001.

Parameters	Estimate (se)
β (Dimension_i)	
Dimension X	-5.56 (0.54)
Dimension Y	-5.43 (0.54)
Dimension Z	-7.42 (0.54)
γ (Net_i, Run_i)	
Light net, Run I	3.29 (0.69)
Light net, Run II	0 (0)
Heavy net, Run I	-0.19 (0.54)
Heavy net, Run II	-0.34 (0.59)

Accepted manuscript



Fig. 1. The observation unit.

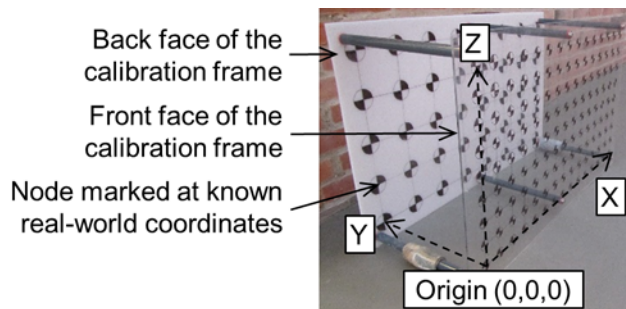


Fig. 2. The calibration frame.

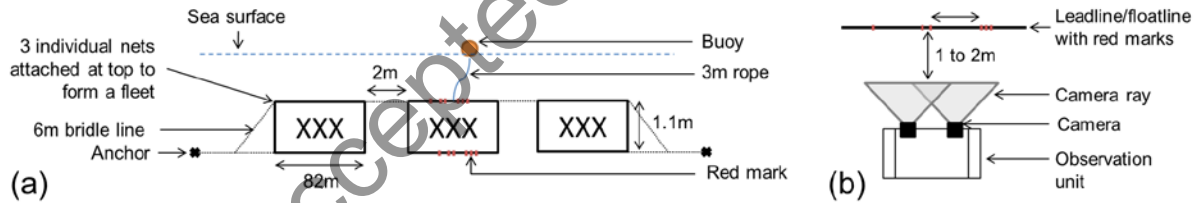


Fig. 3. Experimental set-up for stereo imaging with (a) side view of a fleet, i.e., a ganged sequence of 3 individual gillnets, set on the bottom, (b) top view of the observation unit positioned in front of a net.

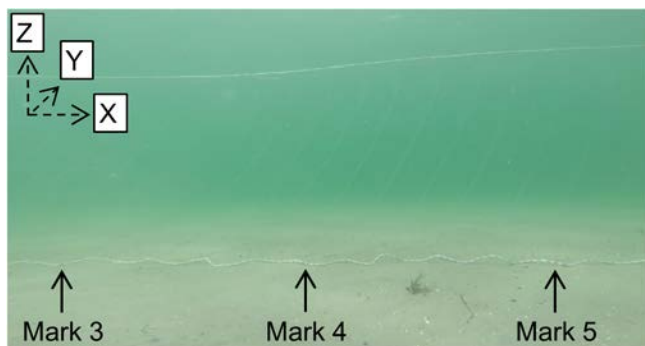


Fig. 4. An in situ example (fleet Ic) of the positions of three different marks (identified from 3 to 5) on the leadline of the same net recorded in the three dimensions (X, Y and Z).

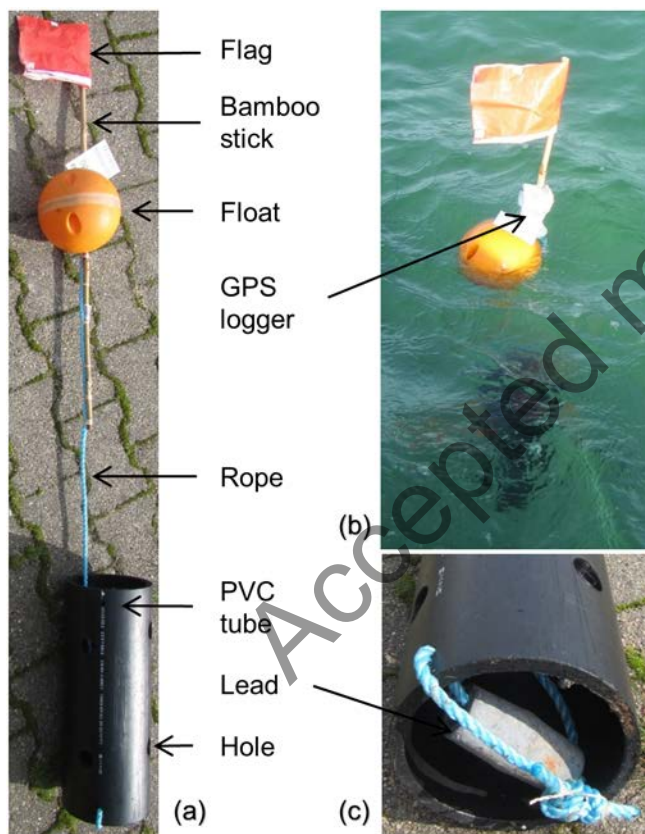


Fig. 5. Drifting device to measure current speed and direction with (a) full view of the device, (b) view of the device at sea, and (c) close-up view of the lower end of the PVC tube which allows to measure at the median net height in the water column. Two similar devices were left drifting between the nets during data collection.

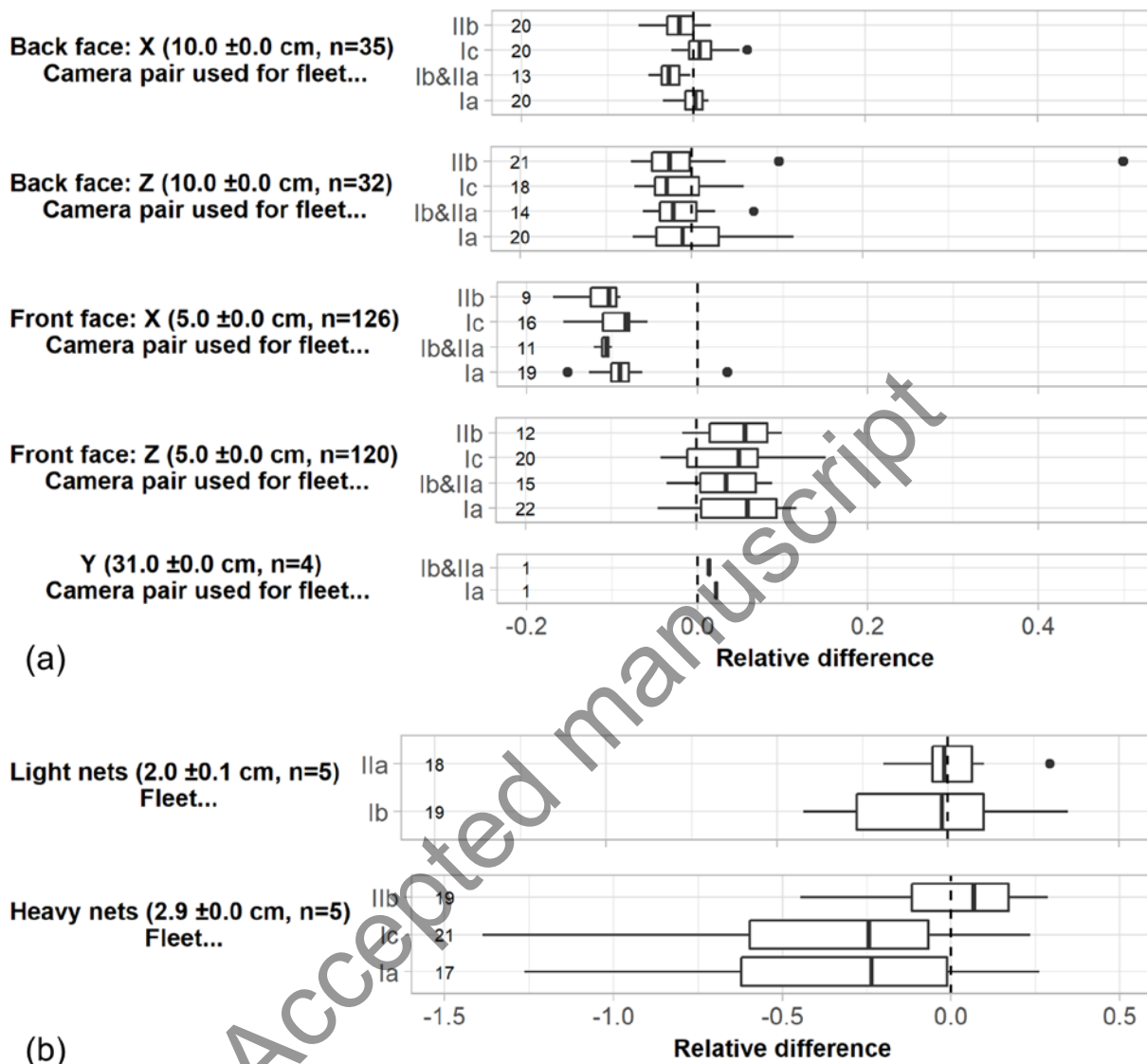


Fig. 6. (a) Relative difference of the calculated distances (with Vidsync) compared to the measured distances (with a measuring tape) between two nodes of the calibration frame on the back and front faces in the X (horizontal) and Z (vertical) dimensions, and between the back and front faces of the calibration frame (Y). (b) Relative difference of the calculated distances (with Vidsync) compared to the measured distances (with a measuring tape) between two coloured threads on the leadline of light and heavy bottom gillnets. On both (a) and (b), the horizontal

dashed line stands for reference as no difference between measured and calculated. The distances measured are given as an average \pm standard deviation with n the number of observations on the left of each plot. The number of the calculated distances used for the comparison is given on the right of each corresponding boxplot.

Accepted manuscript

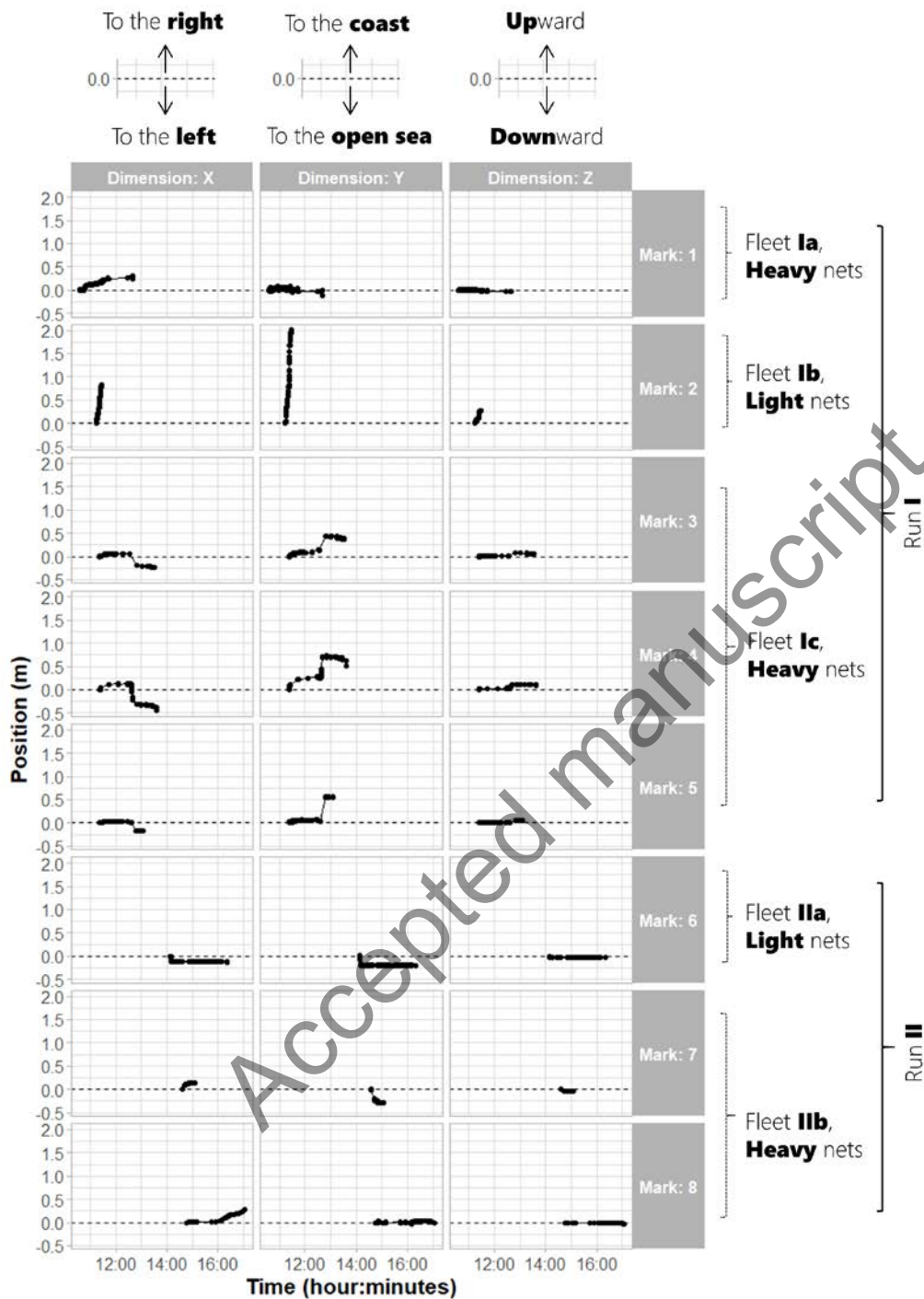


Fig. 7. Time plot of the relative position of the eight marks on the leadline of light and heavy gillnets observed in the pilot sea trial, in the X, Y and Z dimensions. The relative position is given in m as the distance from the initial position (horizontal dashed line). Time is given as the real time of the day in hour:minutes.

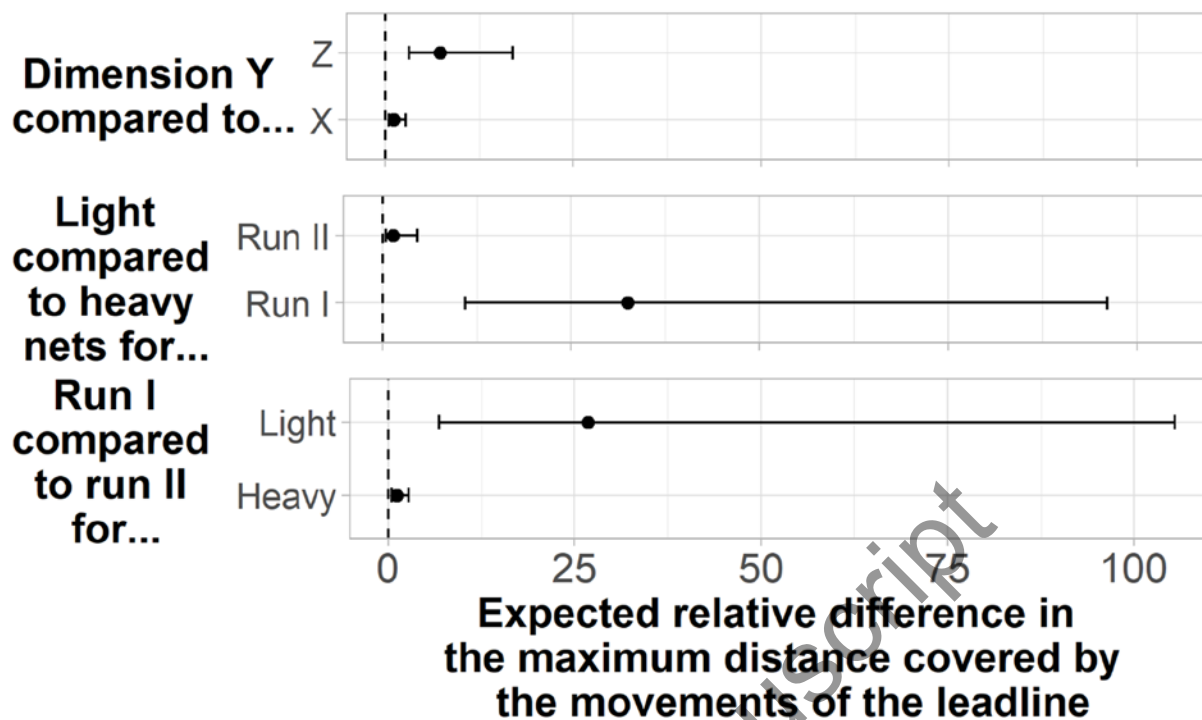


Fig. 8. Expected relative difference (95% confidence limits) in the maximum distance covered by the movements of the leadline for the different experimental configurations.

Accepted manuscript